



**HAL**  
open science

# Large-eddy simulation of turbulent channel flow using relaxation filtering: Resolution requirement and Reynolds number effects

François Kremer, Christophe Bogey

► **To cite this version:**

François Kremer, Christophe Bogey. Large-eddy simulation of turbulent channel flow using relaxation filtering: Resolution requirement and Reynolds number effects. *Computers and Fluids*, 2015, 116, pp.17-28. 10.1016/j.compfluid.2015.03.026 . hal-02060460

**HAL Id: hal-02060460**

**<https://hal.science/hal-02060460>**

Submitted on 4 Jul 2024

**HAL** is a multi-disciplinary open access archive for the deposit and dissemination of scientific research documents, whether they are published or not. The documents may come from teaching and research institutions in France or abroad, or from public or private research centers.

L'archive ouverte pluridisciplinaire **HAL**, est destinée au dépôt et à la diffusion de documents scientifiques de niveau recherche, publiés ou non, émanant des établissements d'enseignement et de recherche français ou étrangers, des laboratoires publics ou privés.

## Accepted Manuscript

Large-eddy simulation of turbulent channel flow using relaxation filtering: resolution requirement and Reynolds number effects

Francois Kremer, Christophe Bogey

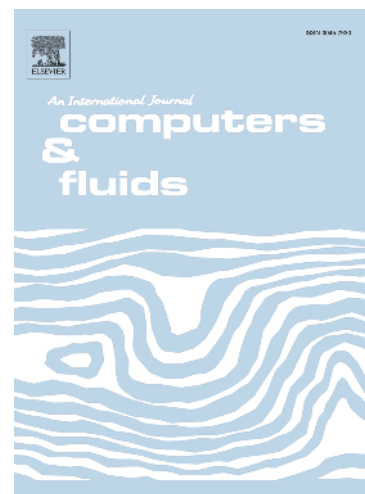
PII: S0045-7930(15)00099-7  
DOI: <http://dx.doi.org/10.1016/j.compfluid.2015.03.026>  
Reference: CAF 2845

To appear in: *Computers & Fluids*

Received Date: 28 March 2014  
Revised Date: 12 March 2015  
Accepted Date: 29 March 2015

Please cite this article as: Kremer, F., Bogey, C., Large-eddy simulation of turbulent channel flow using relaxation filtering: resolution requirement and Reynolds number effects, *Computers & Fluids* (2015), doi: <http://dx.doi.org/10.1016/j.compfluid.2015.03.026>

This is a PDF file of an unedited manuscript that has been accepted for publication. As a service to our customers we are providing this early version of the manuscript. The manuscript will undergo copyediting, typesetting, and review of the resulting proof before it is published in its final form. Please note that during the production process errors may be discovered which could affect the content, and all legal disclaimers that apply to the journal pertain.



# Large-eddy simulation of turbulent channel flow using relaxation filtering: resolution requirement and Reynolds number effects

Francois Kremer\* and Christophe Bogey†

*Laboratoire de Mécanique des Fluides et d'Acoustique, UMR CNRS 5509,  
Ecole Centrale de Lyon, Université de Lyon, 69134 Ecully Cedex, France*

April 10, 2015

## Abstract

Large-eddy simulations (LES) of fully developed channel flows are performed using relaxation filtering as a subgrid-scale model in order to investigate the performance of the LES methodology for wall-bounded flows. For this, LES are carried out using different spatial resolutions, and then for channels flows at different Reynolds numbers. The accuracy of the results is discussed both *a priori* and *a posteriori*, by examining the transfer function of the dissipation mechanisms associated with molecular viscosity and relaxation filtering in the wavenumber space, the quality of the discretization of the dominant turbulent scales based on velocity snapshots and integral length scales, the convergence of the velocity profiles with respect to the grid, and their consistency with data from Direct Numerical Simulation of the literature. In the first step, a channel flow at a friction-velocity-based Reynolds number  $Re_\tau = 300$  is computed using fourteen grids with mesh spacings  $15 \leq \Delta x^+ \leq 45$  in the streamwise direction,  $0.5 \leq \Delta y^+ \leq 4$  at the wall in the wall-normal direction, and  $5 \leq \Delta z^+ \leq 15$  in the spanwise directions, in wall units. A very good accuracy is obtained for  $\Delta x^+ = 30$ ,  $\Delta y^+ = 1$  and  $\Delta z^+ = 10$ . In the second step, three channel flows at Reynolds numbers  $Re_\tau = 350$ , 600 and 960 are simulated using grids with mesh spacings smaller than, or equal to the mesh spacings reported above. The results are shown to be reliable, and demonstrate that the Reynolds number effects are well captured in the present LES of wall-bounded turbulent flows.

*Keywords* : large-eddy simulation, relaxation filtering, channel flow, spatial resolution, Reynolds number

---

\*PhD, now at *CSSI, 545 avenue Augustin Fresnel, 13100 Aix-en-Provence, Email: kremer.francois@gmail.com*

†CNRS Research Scientist, Email: christophe.bogey@ec-lyon.fr

## 1 Introduction

Over the last two decades, computational fluid dynamics has become an efficient tool for the study of wall turbulence. In particular, wall-bounded flows at ever-higher Reynolds numbers have been simulated, which enabled the effects of the Reynolds number on flow statistics and coherent structures to be discussed [1]. It remains, however, difficult to reproduce the features of wall-bounded flows numerically, because wall turbulence is strongly influenced by the dynamics of the small scales developing close to the wall, which exhibit strong anisotropy and complex interactions with larger scales. These small scales must therefore be accurately calculated in simulations. This has been done in most cases using Direct Numerical Simulation (DNS) for channel flows [2, 3, 4, 5, 6, 7, 8] and boundary layers [9, 10, 11, 12, 13]. Unfortunately, as the Reynolds number increases, the computational cost of a DNS is rapidly prohibitive. As an illustration, note for instance that twenty years have elapsed between the DNS by Kim *et al.* [2] and by Hoyas *et al.* [8] for channel flows at Reynolds numbers differing by one decade only.

In order to reduce the numerical cost, Large Eddy Simulations (LES), in which only the largest eddies are resolved, can be used. The effects of the under-resolved eddies are then taken into account by a so-called subgrid-scale model, which classically relies on the assumptions that the large scales carry energy, and that the small scales have mainly dissipative effects [14]. Depending on the possible near-wall resolution, wall-modelled or wall-resolved LES can be performed. In the first approach, only the outer part of wall-bounded flows is resolved, whereas the inner part is modelled [15]. In this way, very high Reynolds numbers can be reached [16], but the near-wall structures are not captured. In the second approach, both the outer and inner parts of the flows are computed at the expense of the computational cost. Accordingly, the range of Reynolds numbers affordable with wall-resolved LES is much smaller, and falls within the range of Reynolds numbers considered in DNS [17, 18, 19, 20]. The cost is however significantly lower using LES. For example, the number of grid points is about 10 times smaller in the LES of a boundary layer performed by Schlatter *et al.* [20] than in a DNS.

In wall-resolved LES, various numerical parameters such as the inflow and boundary conditions, the grid resolution, the subgrid-scale model and the discretization schemes can affect the calculation of the near-wall turbulent structures. It is consequently necessary to validate the simulation methods carefully. Regarding the impact of the inflow conditions, for example, Schlatter & Örlü [13] have reviewed data from several DNS of boundary layers, and pointed out

some differences in basic integral quantities and in flow statistics. They showed in particular that flow features are significantly influenced by the inflow parameters and the boundary-layer tripping [21]. Such difficulties do not exist for fully-developed channel flows, where periodic conditions are imposed in the streamwise direction where turbulence is homogeneous. It appears therefore particularly interesting to study the quality of the LES of wall-bounded flows by simulating channel flows. This is the case for instance in the papers by Rasam *et al.* [22] and by Vuorinen *et al.* [23], who examined the effects of subgrid-scale model and grid resolution, and of a space discretization method, respectively.

In the present work, turbulent channel flows are simulated by LES using relaxation filtering as a subgrid-scale model. This LES approach was proposed by Visbal & Rizzetta [24], Mathew *et al.* [25] and Bogey & Bailly [26], among others. It consists in filtering the flow variables every  $n$ -th time step using a high-order low-pass filter at a strength  $\sigma$  between 0 and 1, in order to relax turbulent energy from the smallest discretized scales, characterized by wave numbers close to the grid cut-off wave number, while leaving larger scales mostly unaffected. In practice, the filtering is usually applied every time step at a fixed strength  $\sigma \simeq 1$  in order to ensure numerical stability, which is not guaranteed when low-dissipation and/or centered discretization schemes are used. Note, however, that dynamic procedures can be built to adjust the parameters of the filtering to the flow characteristics, e.g. in Tantikul & Domaradzki [27]. In previous studies, the validity of the LES approach was explored for a Taylor-Green vortex flow [28], free shear layers [29] and jets [26, 30, 31, 32]. The approach has also been successfully employed for a flow around an airfoil [33] or for a turbulent boundary layer [19]. Here, the performance of the LES method is investigated for wall-bounded flows by simulating fully developed channel flows on grids at different spatial resolutions and for different Reynolds numbers. The first objective is to determine for which mesh spacings accurate results, converged with respect to the grid, can be obtained. The second one is to check that Reynolds number effects [30, 34] on wall turbulence are reproduced. For this, velocity profiles and spectra obtained near the wall, and in particular in the buffer-layer region, where small scales play an important role, will be presented, and comparisons with DNS data of the literature will be provided. Transfer functions associated with molecular viscosity and relaxation filtering will also be shown in the wavenumber space.

The paper is organized as follows. The LES performed for a channel flow at different spatial resolutions are presented in section 2. The LES of channel flows at different Reynolds numbers are reported in section 3. Finally, concluding remarks are given in section 4.

## 2 LES of a turbulent channel flow at different spatial resolutions

### 2.1 Parameters

Large-eddy simulations of a turbulent channel flow are performed by solving the three-dimensional compressible Navier-Stokes equations on Cartesian meshes. The channel flow is at a Reynolds number of  $Re_\tau = u_\tau h / \nu = 300$  and a Mach number of  $M = U_0 / c = 0.4$ , where  $U_0$  is the centerline velocity,  $c$  is the speed of sound,  $h$  is the channel half-width,  $u_\tau = \sqrt{\tau_w / \rho}$  is the friction velocity,  $\tau_w$  is the wall shear stress, and  $\nu$  and  $\rho$  are the kinematic molecular viscosity and the density of the flow. The streamwise, wall-normal and spanwise coordinates are denoted by  $x$ ,  $y$  and  $z$ , respectively. The sizes of the computational domain in the streamwise, wall-normal and spanwise directions are  $L_x = 12h$ ,  $L_y = 2h$  and  $L_z = 6h$ . The walls of the channel are located at  $y = 0$  and  $y = 2h$ , where a no-slip condition is imposed. Periodic boundary conditions are implemented in the  $x$  and  $z$  directions. The spatial derivatives are computed using an explicit 4th-order 11-point redcentered finite-difference scheme [35]. Time integration is performed with an explicit 4th-order 6-step Runge-Kutta algorithm [36]. An explicit 6th-order 11-point redcentered filter [37] is applied every time iteration to the density, momentum and pressure variables with a strength  $\sigma = 1$  in order to remove spurious grid-to-grid oscillations, whose wavelength is equal to twice the mesh spacing, and to relax subgrid-scale energy. Since centered finite differences and a low-dissipation time integration scheme are used, the filtering is necessary to ensure numerical stability.

It is applied sequentially in the three spatial directions  $x$ ,  $y$  and  $z$ . The filtering of the variable  $\varphi$  in the direction  $\alpha$  yields, for instance, the following filtered variable

$$\tilde{\varphi}(\alpha_i) = \varphi(\alpha_i) - \sigma D(\varphi)|_i \quad (1)$$

where  $\alpha_i$  is the coordinate of the  $i^{\text{th}}$  grid point, and  $D$  is the filtering operator

$$D(\varphi)|_i = \sum_{j=-N}^N d_j \varphi(\alpha_{i+j}) \quad (2)$$

based on the filter coefficients  $d_j$ . The damping function  $D^* = \mathcal{F}(D)$  in the Fourier space of the filter used in the present LES is represented in figure 1 as a function of the wavenumber  $k$  normalized by the grid spacing  $\Delta$ . It is equal to 1 for the highest wavenumber taken into account by the grid, namely  $k\Delta = \pi$ , corresponding to  $\lambda = 2\Delta$ , whereas it is smaller than  $10^{-2}$

for  $k\Delta \lesssim \pi/2$ , and even than  $10^{-5}$  for  $k\Delta \lesssim \pi/4$ . Therefore, the grid-to-grid oscillations are completely removed by the filtering, whereas the larger scales are very weakly affected.

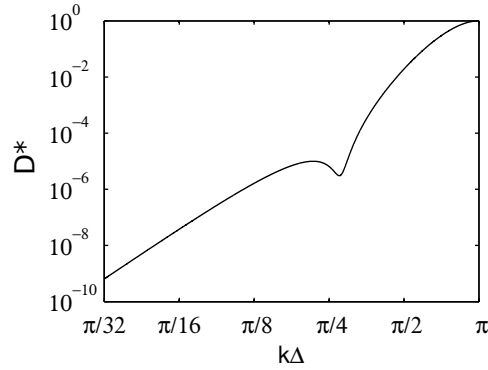


Figure 1. Damping function of the explicit 6th-order 11-point filter [37] used for the relaxation filtering, as a function of the normalized wavenumber  $k\Delta$ , where  $\Delta$  is the grid spacing.

The influence of the spatial resolution is examined by performing fourteen simulations on grids with different mesh spacings, which are given in table 1 in wall units. In all cases, the mesh spacings in the streamwise and spanwise directions,  $\Delta x$  and  $\Delta z$ , are constant. On the contrary, the mesh spacing in the wall-normal direction is stretched from the wall at an expansion ratio  $r \simeq 4\%$  in order to save computational time. The mesh spacings at the wall and at the center of the channel are denoted by  $\Delta y_w$  and  $\Delta y_c$ , respectively. The effects of the mesh spacing in the  $x$ ,  $y$  and  $z$  directions are investigated by considering three sets of grids. In the five grids referred to as gridX45, gridX35, gridX30, gridX25 and gridX15, the mesh spacings are  $\Delta y_w^+ = 0.95$ ,  $\Delta y_c^+ = 15$  and  $\Delta z^+ = 7.5$ , whereas  $\Delta x^+$  decreases from 45 down to 15. In gridY4, gridY2, gridY1 and gridY0.5, they are equal to  $\Delta x^+ = 15$ ,  $\Delta y_c^+ = 15$ ,  $\Delta z^+ = 7.5$ , whereas the mesh spacing at the wall in the  $y$  direction reduces from  $\Delta y_w^+ = 3.7$  to 0.47. Finally, in gridZ15, gridZ12.5, gridZ10, gridZ7.5 and gridZ5, the mesh spacings are  $\Delta x^+ = 15$ ,  $\Delta y_w^+ = 0.95$ ,  $\Delta y_c^+ = 15$ , and  $\Delta z^+ = 15$ , 12.5, 10, 7.5 and 5. Note that gridX15, gridY1 and gridZ7.5 are one and the same case. For the comparison, the mesh spacings in the LES of a channel flow performed by Viazzo *et al.* [17], and in the LES of turbulent boundary layers carried out by Gloerfelt & Berland [19] and by Schlatter *et al.* [20] are reported in table 1. The mesh spacings in the DNS of Kim *et al.* [2], Moser *et al.* [3], del Alamo *et al.* [6] and Hu *et al.* [7] are also given. They are significantly larger in the LES than in the DNS, especially at the wall where the normal mesh spacings are around  $\Delta y_w^+ = 1$  in the former case, but close to or smaller than  $\Delta y_w^+ = 0.1$  in the latter.

Concerning the number of points in the present grids, it varies because of the fixed sizes of the computation domain, yielding  $87 \leq n_x \leq 257$ ,  $85 \leq n_y \leq 161$  and  $129 \leq n_z \leq 385$ . In each

case, the time step  $\Delta t$  is chosen such that  $CFL_y = c\Delta t/\Delta y_w = 0.8$  is obtained, ensuring the stability of the explicit time integration.

Table 1. Parameters of the grids used for the LES of the channel flow at  $Re_\tau = 300$  and for LES redand DNS in the literature: mesh spacings  $\Delta x^+$  in the  $x$  direction,  $\Delta y_w^+$  and  $\Delta y_c^+$  in the  $y$  direction at the wall and at the center of the channel, and  $\Delta z^+$  in the  $z$  direction, in wall units; stretching ratio  $r$  of the mesh spacing in the  $y$  direction.

case	$\Delta x^+$	$\Delta y_w^+$	$\Delta y_c^+$	$\Delta z^+$	$r$ (%)
gridX45	45	0.95	15	7.5	4.4
gridX35	35	0.95	15	7.5	4.4
gridX30	30	0.95	15	7.5	4.4
gridX25	25	0.95	15	7.5	4.4
gridX15	15	0.95	15	7.5	4.4
gridY4	15	3.7	15	7.5	3.5
gridY2	15	1.9	15	7.5	4.0
gridY1	15	0.95	15	7.5	4.4
gridY0.5	15	0.47	15	7.5	4.5
gridZ15	15	0.95	15	15	4.4
gridZ12.5	15	0.95	15	12.5	4.4
gridZ10	15	0.95	15	10	4.4
gridZ7.5	15	0.95	15	7.5	4.4
gridZ5	15	0.95	15	5	4.4
redLES of Viazzo <i>et al.</i> [17]	31.4	0.88	51.84	15.7	
redLES of Gloerfelt & Berland [19]	37	0.98		14.7	2
redLES of Schlatter <i>et al.</i> [20]	25.3	<1	14.2	10.8	
redDNS of Kim <i>et al.</i> [2]	12	0.05	4.4	7	
redDNS of Moser <i>et al.</i> [3] at $Re_\tau = 395$ and 590	$\leq 10$	$\leq 0.04$	$\leq 7.2$	$\leq 6.5$	
redDNS of del Alamo <i>et al.</i> [6] at $Re_\tau = 950$	7.6	0.03	7.6	3.8	
redDNS of Hu <i>et al.</i> [7]	16.88	$\leq 0.12$	$\leq 9.42$	8.44	

## 2.2 Dissipation transfer functions

In this section, the quality of the present LES is assessed *a priori* by comparing the contributions of the dissipation mechanisms, namely molecular viscosity and relaxation filtering, in the simulations. For that purpose, their respective transfer functions are plotted against the normalized wavenumber  $k\Delta$ , where  $\Delta$  is the mesh spacing, as proposed in Bogey *et al.* [32]. These functions, when multiplied by the turbulent energy spectrum  $E(k)$ , provide the spectral density of energy dissipation. For molecular viscosity, the latter quantity is known to be  $\nu k^2 E(k)$  yielding a transfer function equal to  $\nu k^2$ , and to  $\nu(k\Delta)^2/\Delta^2$  when expressed as a function of the normalized wavenumber  $k\Delta$ . For the relaxation filtering applied every time step, the transfer function is found to be  $\sigma D^*(k\Delta)/\Delta t$ , where  $D^*(k\Delta)$  is the damping function of the filter defined and plotted in previous section, and  $\sigma$  is the filtering strength. In the LES, the key issue is to determine whether, given a specific mesh spacing, the scales well calculated by the numerical



methods, which here are the scales discretized by at least 5 points per wavelength, are mainly dissipated by viscosity or by the relaxation filtering. The second case is not desirable because it may result in the excessive damping of the largest turbulent scales and in the artificial reduction of the effective flow Reynolds number [30].

The transfer functions are calculated for the simulations performed using gridX meshes, including gridX15 also known as gridY1 and gridZ7.5, with  $\Delta y_w^+ = 0.95$  at the wall and a time step  $\Delta t = 0.8\Delta y_w/c$ . They are represented in figure 2 as a function of the normalized wavenumber  $k\Delta$ , for the mesh spacings  $\Delta^+ = 7.5, 15, 30$  and  $45$ , in wall units. These values are chosen because  $\Delta^+ = 7.5$  and  $\Delta^+ = 15$  correspond to the mesh spacings in the  $z$  direction and in the  $y$  direction at the center of the channel, and  $\Delta^+ = 15, 30$  and  $45$  are equal to the mesh spacing in the  $x$  direction using gridX15, gridX30 and gridX45, respectively. One curve is obtained for the relaxation filtering, whose normalized transfer function does not depend on the mesh spacing. On the contrary, four curves are found for the transfer function associated with molecular viscosity, which varies as  $1/\Delta^2$ , and consequently moves upwards with decreasing  $\Delta$  or increasing grid resolution.

For  $\Delta^+ = 7.5$ , the transfer function associated with molecular viscosity is above that of the relaxation filtering for  $k\Delta < 1.1$ , and below for  $k\Delta > 1.1$ . This indicates that the wavelengths discretized by more than  $\lambda/\Delta = 2\pi/1.1 = 5.7$  points are mainly dissipated by viscosity, whereas the shorter wavelengths are damped by the filtering. For  $\Delta^+ = 15$ , a similar behaviour is noticed, with two transfer functions intersecting at  $k\Delta = 1.0$ , or  $\lambda/\Delta = 6.3$ . For these two grid resolutions, the well-calculated scales are therefore mainly affected by viscous dissipation, and not by the subgrid dissipation provided by the relaxation filtering. For  $\Delta^+ = 30$ , the transfer function of molecular viscosity is higher than that of the filtering for wavenumbers  $k\Delta < 0.48$ . For higher wavenumbers, the two transfer functions are relatively close up to the value  $k\Delta = 0.95$ , from which that of the filtering predominates. For  $\Delta^+ = 45$ , similarly, the transfer function of molecular viscosity is above that of the filtering for  $k\Delta < 0.35$ , and below for  $k\Delta > 0.35$ . This suggests that for  $\Delta^+ = 30$  and  $45$ , the well-calculated scales characterized by wavelengths  $\lambda/\Delta = 2\pi/0.48 < 13$  and  $\lambda/\Delta = 2\pi/0.35 < 18$ , respectively, are significantly damped by the filtering.

The dynamics of the turbulent scales computed in the LES using gridX30 and gridX45 with  $\Delta x^+ = 30$  and  $45$  can consequently be expected to be governed not only by the physical mechanisms associated with molecular viscosity, but also by the relaxation filtering. This does

not appear, however, to be the case using gridX15 and gridX25 in which the mesh spacings in the three spatial directions satisfy  $\Delta^+ < 30$ .

In the two other sets of simulations carried out using gridY and gridZ meshes, the mesh spacings are all smaller than 15 wall units. Based on the results above, this should ensure that the scales well calculated in these LES are not dissipated by the filtering.

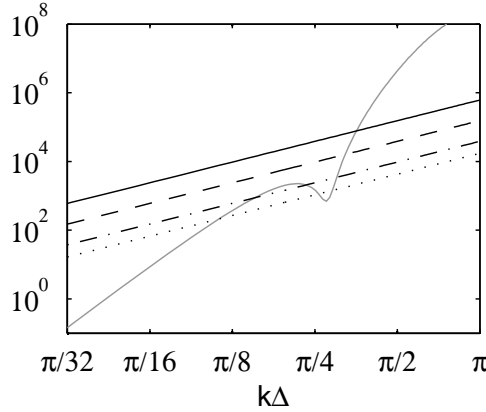


Figure 2. Representation of the dissipation transfer functions obtained for a mesh spacing  $\Delta$  in the LES of the channel flow at  $Re_\tau = 300$  using a time step  $\Delta t = 0.8\Delta y_w/c$  with  $\Delta y_w^+ = 0.95$ , as a function of the normalized wavenumber  $k\Delta$ : grit relaxation filtering, and molecular viscosity for  $\Delta^+ = 45$ ,  $\Delta^+ = 30$ ,  $\Delta^+ = 15$ ,  $\Delta^+ = 7.5$ .

### 2.3 Flow visualisation

Following the *a priori* study of the LES quality, suggesting that some of the LES in this work may not be accurate, the simulation results are now analyzed *a posteriori* in order to assess their convergence with respect to the grid resolution. This point is first discussed qualitatively by visualising the turbulent structures developing close to the wall in the buffer layer, which must be correctly computed in the LES of wall-bounded flows as mentioned in the introduction.

For this, snapshots of velocity fluctuations in a plane at a distance to the wall of  $y^+ = 16$  are examined for the LES using gridZ5, gridX45 and gridZ15. The first grid is the finest grid with  $\Delta x^+ = 15$  and  $\Delta z^+ = 5$ . The two others are the coarsest grids in the streamwise and the spanwise directions, respectively, with  $\Delta x^+ = 45$  in the first case and  $\Delta z^+ = 15$  in the second case, which may lead to the insufficient discretization of the flow turbulent structures.

Streamwise and wall-normal velocity fluctuations obtained using gridZ5 with  $\Delta x^+ = 15$ ,  $\Delta y_w^+ = 0.95$  and  $\Delta z^+ = 5$  are represented in figures 3(a) and 3(b). In the streamwise velocity field, elongated structures are found, coloured in black and grey indicating low-speed and high-speed fluid. These structures correspond to high-speed and low-speed streaks [39], which are

approximately 1000 wall units long and 100 wall units wide. In the wall-normal velocity field, a great number of structures consisting in pairs of black and grey regions elongated in the streamwise direction, where black and grey denote fluid moving toward the wall and away from the wall, are noted. These structures are induced by quasi-streamwise vortices [39], which are from 200 to 400 wall units in length and about 50 wall units in diameter. The turbulent structures observed in figure 3 have sizes which are substantially larger than the mesh spacings. They are consequently well discretized by the grid. Furthermore, these structures look very similar to those in the velocity snapshots obtained using DNS by Jiménez [40] at  $y^+ = 16$  for a channel flow at  $Re_\tau \simeq 1000$ . The LES using gridZ5 therefore seems to be well resolved at the wall.

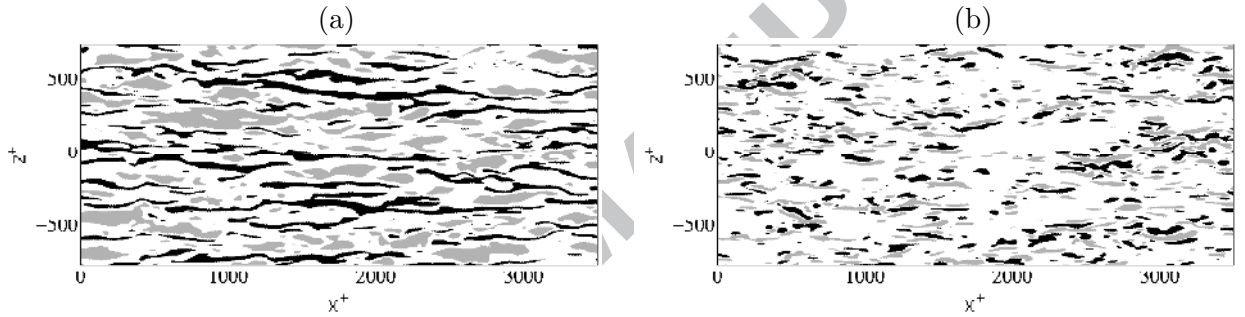


Figure 3. Snapshots of streamwise and wall-normal velocity fluctuations  $u$  and  $v$  obtained at the same time at  $y^+ = 16$  using gridZ5 where  $\Delta x^+ = 15$ ,  $\Delta y_w^+ = 0.95$  and  $\Delta z^+ = 5$ : (a) streamwise velocity (black:  $u < U - u_{rms}$ , white:  $U - u_{rms} < u < U + u_{rms}$ , grey:  $u > U + u_{rms}$ , where  $U$  is the mean streamwise velocity), (b) wall-normal velocity (black:  $v < -v_{rms}$ , white:  $-v_{rms} < v < v_{rms}$ , grey:  $v > v_{rms}$ ).

Snapshots of velocity fluctuations provided by the LES using gridX45 with  $\Delta x^+ = 45$ ,  $\Delta y_w^+ = 0.95$  and  $\Delta z^+ = 7.5$  are shown in figure 4. Compared to the results obtained with  $\Delta x^+ = 15$  in figure 3, there are less differences for the streamwise velocity in figure 4(a) than for the spanwise velocity in figure 4(b). In the former case, similar high-speed and low-speed streaks are found, which can be explained by the fact that they remain much longer than the streamwise mesh spacing  $\Delta x^+ = 45$ . In the latter case, on the contrary, the turbulent structures are more numerous and longer than those in figure 3(b), and have lengths typically between 400 to 500 wall units. The quasi-streamwise vortices developing close to the wall thus appear to be poorly resolved by the grid.

Finally, snapshots of velocity fluctuations given by the LES using gridZ15 where  $\Delta x^+ = 15$ ,  $\Delta y_w^+ = 0.95$  and  $\Delta z^+ = 15$  are displayed in figure 5. The streaks and the quasi-streamwise vortices are up to 200 and 100 wall units wide, respectively. They are wider than those obtained

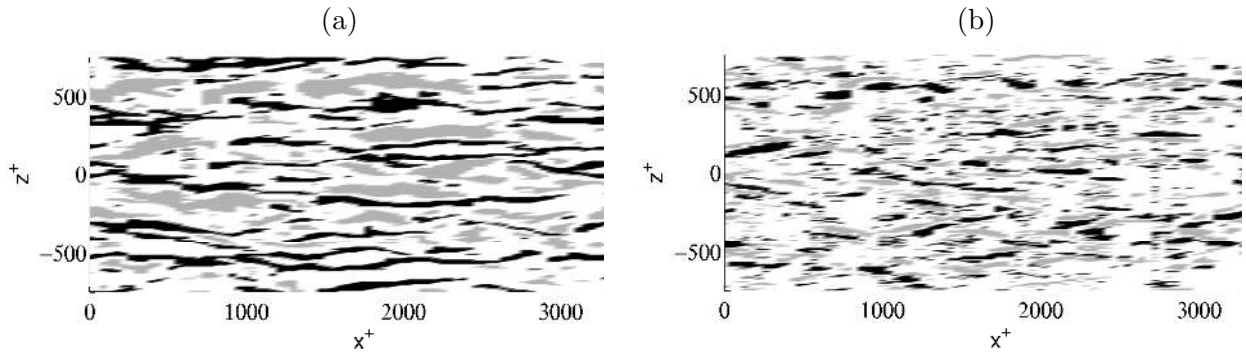


Figure 4. Snapshots of streamwise and wall-normal velocity fluctuations  $u$  and  $v$  obtained at the same time at  $y^+ = 16$  using gridX45 where  $\Delta x^+ = 45$ ,  $\Delta y_w^+ = 0.95$  and  $\Delta z^+ = 7.5$ : (a) streamwise velocity, (b) wall-normal velocity; same color scales as in figure 3.

using  $\Delta z^+ = 5$  in figure 3, indicating that they are insufficiently discretized in the spanwise direction. In particular, the width of quasi-streamwise vortices should be around 50 wall units, which is only about 3 times the spanwise mesh spacing  $\Delta z^+ = 15$ .

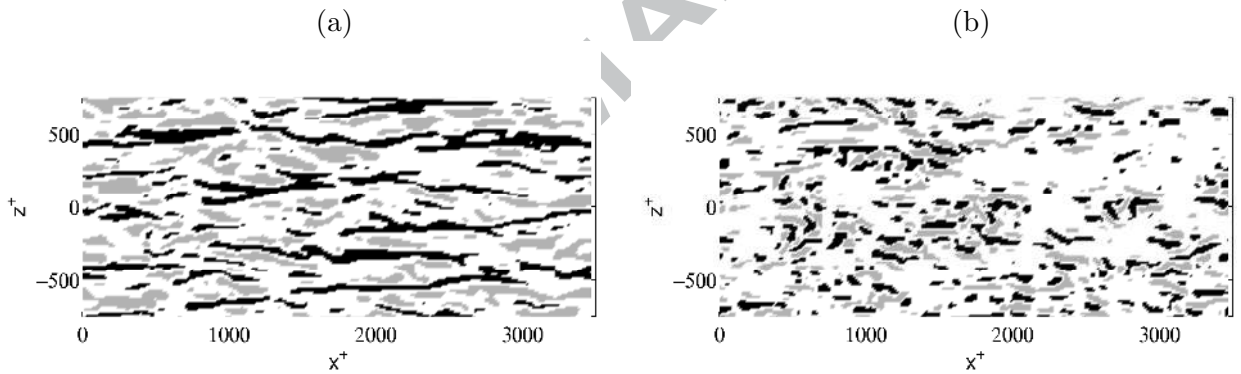


Figure 5. Snapshots of streamwise and wall-normal velocity fluctuations  $u$  and  $v$  obtained at the same time at  $y^+ = 16$  using gridZ15 where  $\Delta x^+ = 15$ ,  $\Delta y_w^+ = 0.95$  and  $\Delta z^+ = 15$ : (a) streamwise velocity, (b) wall-normal velocity; same color scales as in figure 3.

## 2.4 Integral length scales

In order to check the suitability of the LES resolution, characteristic length scales are calculated from the velocity fluctuations in the buffer region, and they are compared to the mesh spacings  $\Delta x$  and  $\Delta z$ . The integral length scales in the streamwise and spanwise directions are defined, respectively, by

$$\begin{cases} L_{uu}^{(x)} = \int_0^\infty \mathcal{R}_{uu}(x, 0) dx \\ L_{uu}^{(z)} = \int_0^\infty \mathcal{R}_{uu}(0, z) dz \end{cases} \quad (3)$$

where

$$\mathcal{R}_{uu}(x, z) = \frac{\overline{u'(x_0, y_0, z_0)u'(x_0 + x, y_0, z_0 + z)}}{\overline{u'^2(y_0)}} \quad (4)$$

is the correlation function obtained for the streamwise velocity fluctuations at the wall distance  $y_0^+ = 16$ . The overbar denotes averaging over time and over all the positions  $(x_0, z_0)$  because turbulence is homogeneous in the  $x$  and  $z$  directions.

In order to obtain reliable values of integral length scales, the correlation functions  $\mathcal{R}_{uu}(x, 0)$  and  $\mathcal{R}_{uu}(0, z)$  are computed from the results obtained with the finest grid, namely gridZ5 with  $\Delta x^+ = 15$ ,  $\Delta y_w^+ = 0.95$  and  $\Delta z^+ = 5$ . They are represented in figure 6 as a function of separation distances normalized by wall units. They both tend to zero as the separation distance increases, as expected. The correlation function in the streamwise direction decreases slowly and monotonically, and becomes smaller than 0.1 for a separation distance of about 600 wall units, which is not shown in the figure. The correlation function in the spanwise direction decreases much faster than the previous one, and presents negative values for  $z^+ \geq 40$ . The integral length scales are then estimated by integrating the correlation functions up to  $x = L_x/2$  for  $\mathcal{R}_{uu}(x, 0)$ , and up to  $z_{max}^+ = 40$  where  $\mathcal{R}_{uu}(0, z_{max}^+) = 0$  for  $\mathcal{R}_{uu}(0, z)$ . Integrating  $\mathcal{R}_{uu}(0, z)$  further in  $z$ , where the function is negative, would indeed artificially reduce the value of  $L_{uu}^{(z)+}$ . Finally, the integral length scales are found to be  $L_{uu}^{(x)+} = 210$  and  $L_{uu}^{(z)+} = 20$ , in wall units.

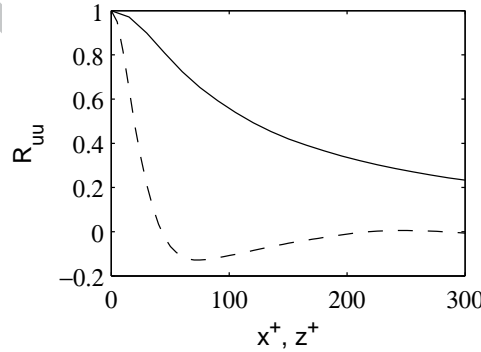


Figure 6. Correlation functions obtained for the streamwise velocity fluctuations  $u$  at  $y^+ = 16$  from the LES using gridZ5 where  $\Delta x^+ = 15$ ,  $\Delta y_w^+ = 0.95$  and  $\Delta z^+ = 5$ :  $R_{uu}(x^+, 0)$  in the  $x$  direction,  $R_{uu}(0, z^+)$  in the  $z$  direction; separation distances in wall units.

The ratios of the integral length scales with different mesh spacings  $\Delta x^+$  between 15 and 45 and  $\Delta z^+$  between 5 and 15 are calculated, and reported in table 2. In the streamwise direction, the ratio  $L_{uu}^{(x)}/\Delta x$  is equal to or larger than 4.6 for all values of  $\Delta x^+$ . In the spanwise direction, on the contrary, the ratio  $L_{uu}^{(z)}/\Delta z$  is only of 4 for  $\Delta z^+ = 5$ , of 2.7 for  $\Delta z^+ = 7.5$  and of 2 or less for  $\Delta z^+ \geq 10$ . Based on these results, and considering from figure 1 that a minimal resolution

of about 4 mesh spacings is required for a proper computation, the grids described in section 2.1 appear fine enough in the streamwise direction, but may be too coarse in the spanwise direction. In particular, for  $\Delta z^+ > 10$ , the spanwise integral length scale is discretized by less than two grid points, which is likely to affect the LES results significantly.

Table 2. Ratios  $L_{uu}^{(x)}/\Delta x$   $L_{uu}^{(z)}/\Delta z$  between the integral length scales obtained from velocity  $u$  at  $y^+ = 16$  in the LES using gridZ5 and mesh spacings for different values of  $\Delta x^+$  and  $\Delta z^+$ .

$\Delta x^+$	$L_x/\Delta x$	$\Delta z^+$	$L_z/\Delta z$
45	4.6	15	1.4
35	6.0	12.5	1.6
30	7.0	10	2.0
25	8.4	7.5	2.7
15	14	5	4.0

## 2.5 Mean and fluctuating velocity profiles

The convergence of the results with respect to the grid is investigated by examining the profiles of mean streamwise velocity  $U^+ = U/u_\tau$  and of rms streamwise velocity fluctuations  $u_{rms}^+ = \sqrt{u'^2}/u_\tau$ , represented as a function of the wall distance  $y^+ = yu_\tau/\nu$ .

The results provided by the LES using gridY4, gridY2, gridY1 and gridY0.5 are shown in figure 7. The velocity profiles obtained with  $\Delta y_w^+ = 3.7, 1.9$  and  $0.95$  differ, whereas those obtained with  $\Delta y_w^+ = 0.95$  and  $0.47$  are very close, which suggests grid convergence for  $\Delta y_w^+ = 0.95$ . It can be noted that in the simulations carried out with  $\Delta y_w^+ = 3.7$  and  $1.9$ , the values of  $U^+$  and  $u_{rms}^+$  are appreciably underestimated. This is particularly the case for the peak value of rms velocity fluctuations in figure 7(b), highlighting the importance of the first grid point in the  $y$  direction near the wall.

The mean and rms velocity profiles obtained in the simulations gridZ where  $\Delta z^+$  varies between 5 and 15 are presented in figure 8. Overall, the profiles do not change much with the spanwise mesh spacing for  $\Delta z^+ \leq 10$ , but discrepancies are observed for  $\Delta z^+ > 10$ , which is in agreement with the conclusions of the analysis of section 2.4. Convergence is thus practically reached for  $\Delta z^+ = 10$ . Moreover, with respect to the well-resolved LES, the values of mean and rms streamwise velocities in the under-resolved LES with  $\Delta z^+ = 12.5$  and  $15$  are overestimated, respectively, in the outer part of the flow and in the buffer region.

The results obtained in the cases gridX with  $15 \leq \Delta x^+ \leq 45$  are plotted in figure 9. For both mean velocity and rms velocity fluctuations, the profiles are very similar for  $\Delta x^+ \leq 30$ , indicating grid convergence, as expected given the results of section 2.2. For  $\Delta x^+ > 30$ , as

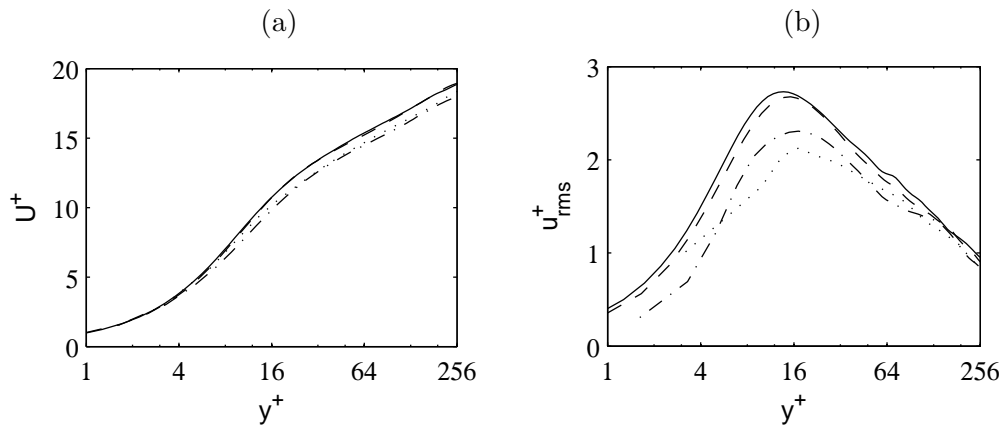


Figure 7. Representation (a) of the mean value and (b) the rms fluctuations of streamwise velocity obtained in the LES using black gridY4, black gridY2, black gridY1, black gridY0.5, as a function of the wall distance using wall units.

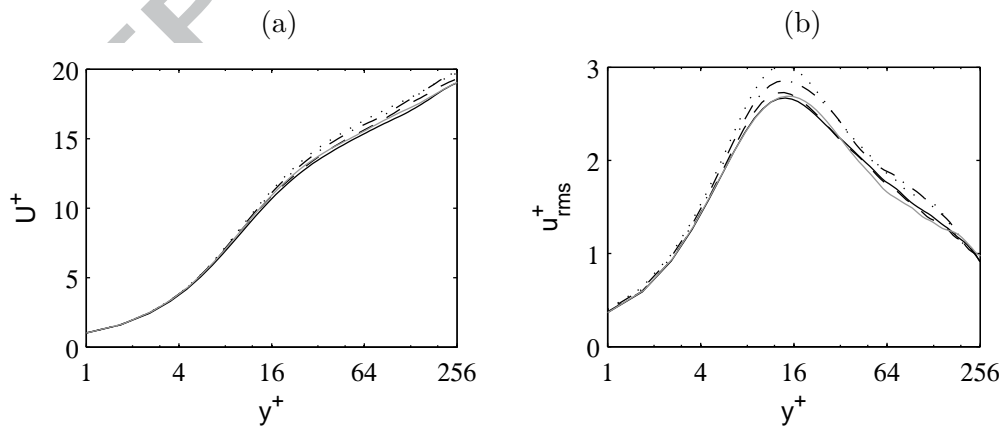


Figure 8. Representation (a) of the mean value and (b) the rms fluctuations of streamwise velocity obtained in the LES using black gridZ15, black gridZ12.5, black gridZ10, black gridZ7.5, gris gridZ5, as a function of the wall distance using wall units.

previously using coarse grids in the  $z$  direction, the values of mean and rms velocities are higher than those found using fine grids.

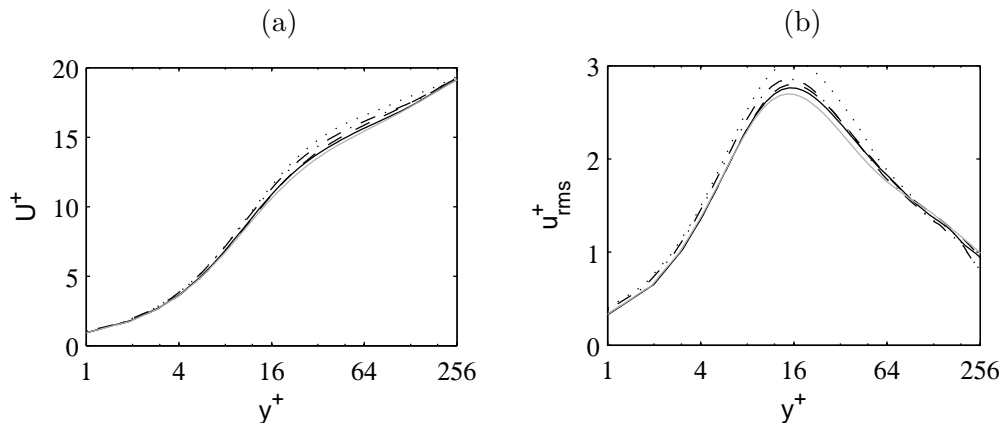


Figure 9. Representation (a) of the mean value and (b) the rms fluctuations of streamwise velocity obtained in the LES using gridX45, gridX35, gridX30, gridX25, gridX15, as a function of the wall distance using wall units.

## 2.6 Spanwise velocity spectra

Spanwise spectra  $\phi_{uu}(k_z)$  of the streamwise velocity fluctuations at  $y^+ = 16$  are computed for the LES performed using gridZ15, gridZ10 and gridZ7.5 with a streamwise mesh spacing  $\Delta x^+ = 15$ , and spanwise mesh spacings  $\Delta z^+ = 15, 10$  and  $7.5$ . They are represented in figure 10 as a function of the spanwise wavenumber  $k_z$ , normalized by wall units. They all slowly increase with wavenumber at low wavenumbers, reach a maximum around a value  $k_z^{max+} = 0.038$  indicated by a vertical grey line. Besides, at high wavenumbers, they exhibit a very sharp decrease beyond  $k_z^+ = 0.07, 0.1$  and  $0.15$ , respectively, for  $\Delta z^+ = 15, 10$  and  $7.5$ . In the three cases, these wavenumbers correspond to wavelengths  $\lambda_z = 2\pi/k_z$  discretized by approximately  $\lambda_z/\Delta z = 6$  points. Therefore, the sharp decreases can be attributed to the effects of the relaxation filtering, which is designed to damp wavelengths shorter than about 5 mesh spacings.

In the three LES, the dominant components in the velocity spectra are centered around  $k_z^{max+} \simeq 0.038$ , yielding  $\lambda_z^{max+} \simeq 166$ . This length scale gives an estimate of the size of the turbulent structures contributing the most to the kinetic energy at the wall. The components on the right side of the peak exhibit lower levels than those on the left side, but they extend over a wider range of wavenumbers, namely from  $k_z^+ = 0.4$  to approximately 1.5 in the LES using gridZ7.5, and thus contribute significantly to the total energy. This wavenumber range is reduced for smaller mesh spacings  $\Delta z^+$ . In particular, it lies between about  $k_z^+ = 0.4$  and  $0.7$



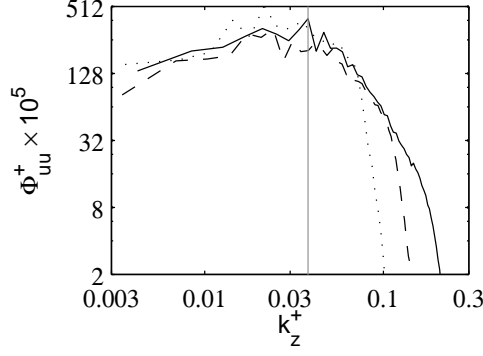


Figure 10. Representation of the power spectral densities of the streamwise velocity fluctuations obtained at  $y^+ = 16$  in the LES using gridZ15, gridZ10, and gridZ7.5, as a function of the spanwise wavenumber  $k_z^+$  using wall units; grid  $k_z^+ = 0.038$ .

for  $\Delta z^+ = 15$ , suggesting that a non-negligible portion of the energy is artificially damped in the LES using gridZ15.

### 3 LES of channel flows at different Reynolds numbers

#### 3.1 Parameters

Three large-eddy simulations of turbulent channel flows at a Mach number of  $M = 0.5$  and at Reynolds numbers of  $Re_\tau = 350, 600$  and  $960$ , referred to as Re350, Re600 and Re960, are performed. The Mach number is slightly higher than the Mach number of  $M = 0.4$  considered in section 2. However, both are low enough so that compressibility effects are very weak, and that the flow features do not appreciably depend on the Mach number [45]. In the three LES, the dimensions of the computational domain are  $L_x \times L_y \times L_z = 12h \times 2h \times 6h$ , where  $h$  is the half-width of the channel. The grids used contain from 8.1 million points for Re350 up to 68 million points for Re960. Their main parameters are given in table 3. In the Re350 case, the mesh spacings in wall units are  $\Delta x^+ = 17$  and  $\Delta z^+ = 8.5$  in the streamwise and spanwise directions, and  $\Delta y_w^+ = 0.97$  at the wall and  $\Delta y_c^+ = 16$  at the center of the channel in the wall-normal direction. In the Re600 and Re960 cases, the streamwise and spanwise mesh spacings are  $\Delta x^+ = 25$  and  $\Delta z^+ = 10$ . They are slightly larger than those in the Re350 case in order to keep computational costs at a reasonable level. In the  $y$  direction, the mesh spacing at the wall is  $\Delta y_w^+ = 0.97$  for Re600, and  $\Delta y_w^+ = 0.93$  for Re960, and the mesh spacing at the center of the channel is  $\Delta y_c^+ = 10$  in both cases. These values are smaller than, or at least equal to the maximal mesh spacings required according to the study conducted in previous section for

a channel flow at  $Re_\tau = 300$ . The same resolution requirements most probably apply to the present LES, because the near-wall properties of channel flows, when scaled by  $\nu$  and  $u_f$ , are nearly independent from the Reynolds number for  $Re_\tau \leq 1000$  [1].

Table 3. LES of channel flows at varying Reynolds numbers  $Re_\tau$ : Mach number  $M$ , number of grid points  $n_x \times n_y \times n_z$ , and mesh spacings  $\Delta x^+$  in the  $x$  direction,  $\Delta y_w^+$  and  $\Delta y_c^+$  in the  $y$  direction at the wall and at the center of the channel, and  $\Delta z^+$  in the  $z$  direction, in wall units; stretching ratio  $r$  of the mesh spacing in the  $y$  direction.

case	$Re_\tau$	$M$	$n_x \times n_y \times n_z$	$\Delta x^+$	$\Delta y_w^+$	$\Delta y_c^+$	$\Delta z^+$	$r$ (%)
Re350	350	0.5	$247 \times 133 \times 247$	17	0.97	16	8.5	4.4
Re600	600	0.5	$285 \times 185 \times 355$	25	0.97	10	10	4.4
Re960	960	0.5	$457 \times 261 \times 571$	25	0.93	10	10	4.4

As reported in table 4, time integration in the Re350 simulation is performed using an explicit fourth-order six-step Runge-Kutta algorithm [36]. The CFL number  $CFL_y = c\Delta t/\Delta y_w$  at the wall in the wall-normal direction, where  $\Delta t$  is the time step, is equal to 0.8. In the Re600 and Re960 simulations, a semi-implicit third-order six-step Runge-Kutta scheme is used in order to reduce computational time. A detailed description of the scheme can be found in a previous paper [38]. The CFL number  $CFL_z = c\Delta t/\Delta z$  in the spanwise direction is equal to 1.0, yielding a CFL number  $CFL_y = 11$  at the wall. The number of time iterations is  $n_{it} = 480,000$ , 24,000 and 35,000, and the duration of the simulations is  $T_{LES}U_0/h = 490$ , 203 and 165, respectively, for Re350, Re600 and Re960.

Table 4. LES of channel flows at varying  $Re_\tau$ : time integration algorithm, CFL numbers  $CFL_y = c\Delta t/\Delta y_w$  in the  $y$  direction and  $CFL_z = c\Delta t/\Delta z$  in the  $z$  direction, time duration  $T_{LES}$  scaled by the centerline velocity  $U_0$  and the channel half-width  $h$ , number of time iterations  $n_{it}$ .

case	algorithm	$CFL_y$	$CFL_z$	$T_{LES}U_0/h$	$n_{it}$
Re350	explicit RK [36]	0.8	0.1	490	480,000
Re600	semi-implicit RK [38]	11	1.0	203	24,000
Re960	semi-implicit RK [38]	11	1.0	165	35,000

The numerical methods for spatial differentiation and relaxation filtering are identical to those used for the LES of section 2. The spatial derivatives are approximated with an explicit 4th-order 11-point finite-difference scheme [35], while an explicit 6th-order 11-point filter [37] is applied to the flow variables at every iteration with a strength  $\sigma = 1$ .

### 3.2 Dissipation transfer functions

Since the aim is to investigate the possibility of studying Reynolds number effects in turbulent channel flows using LES with relaxation filtering, the magnitude of the dissipative mechanisms

in the simulations are compared in the same way as in section 2.2, in order to ensure that the effective flow Reynolds number is not artificially reduced. The transfer functions associated with molecular viscosity and relaxation filtering are thus computed for the three LES based on the largest mesh spacing, that is  $\Delta x$  in the streamwise direction, yielding  $\nu(k_x \Delta x)^2 / \Delta x^2$  and  $\sigma D^*(k_x \Delta x) / \Delta t$ , respectively. They are represented in figure 11 as a function of the normalized wavenumber  $k_x \Delta x$ . For the Re350 case in figure 11(a), the transfer function associated with viscosity is above that of filtering for  $k_x \Delta x \leq 1.0$ , and below for  $k_x \Delta x \geq 1.0$ . Viscous effects are consequently stronger than the filtering effects for components discretized by more than  $\lambda_x / \Delta x = 2\pi / 1.0 = 6.3$  points per wavelength, and weaker for shorter components. Similarly, in the Re600 and Re960 cases in figures 11(b) and 11(c), viscosity is dominant for components with more than  $\lambda_x / \Delta x = 5.7$  points per wavelength. These results show that in the present simulations, molecular viscosity provides dissipation of most of the large turbulent scales. Reynolds number effects are therefore expected to be well reproduced.

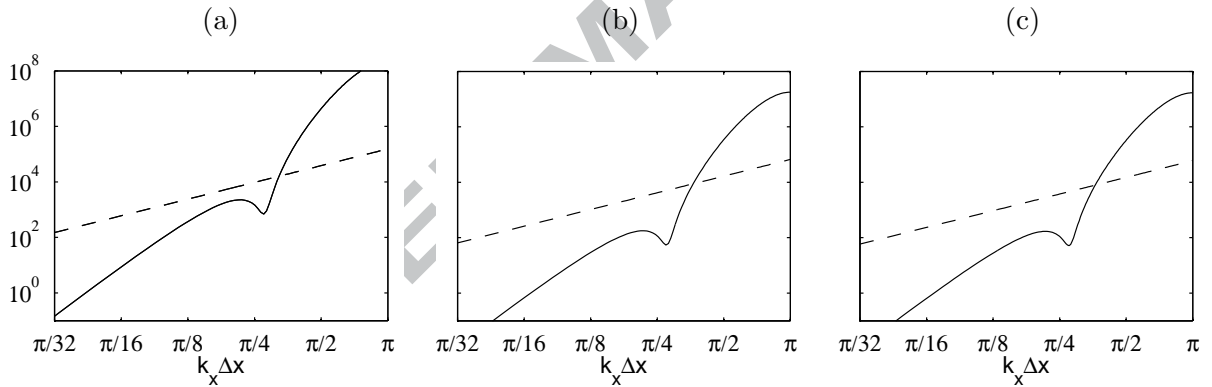


Figure 11. Representation of the dissipation transfer functions obtained in the LES (a) Re350, (b) Re600 and (c) Re960 as a function of the normalized streamwise wave number  $k_x \Delta x$ : relaxation filtering, molecular viscosity.

### 3.3 Flow visualization

In order to illustrate the fine discretization of the near-wall structures in the LES, snapshots of the velocity fluctuations obtained at a distance to the wall of  $y^+ = 18$  are presented in figure 12 for the Re600 and Re960 cases. The results of the former case in figures 12(a,c) and those of the latter in figures 12(b,d) look similar to each other.

For both Reynolds numbers, the streamwise velocity fields in figures 12(a,b) show regions of low-speed and high-speed fluid, elongated in the streamwise direction, corresponding to the near-wall streaks [39]. As for the wall-normal velocity fields in figures 12(c,d), they exhibit a

great number of structures, also elongated in the streamwise direction. These structures are arranged in pairs of regions with fluid moving toward and away from the wall, and they are induced by quasi-streamwise vortices [39].

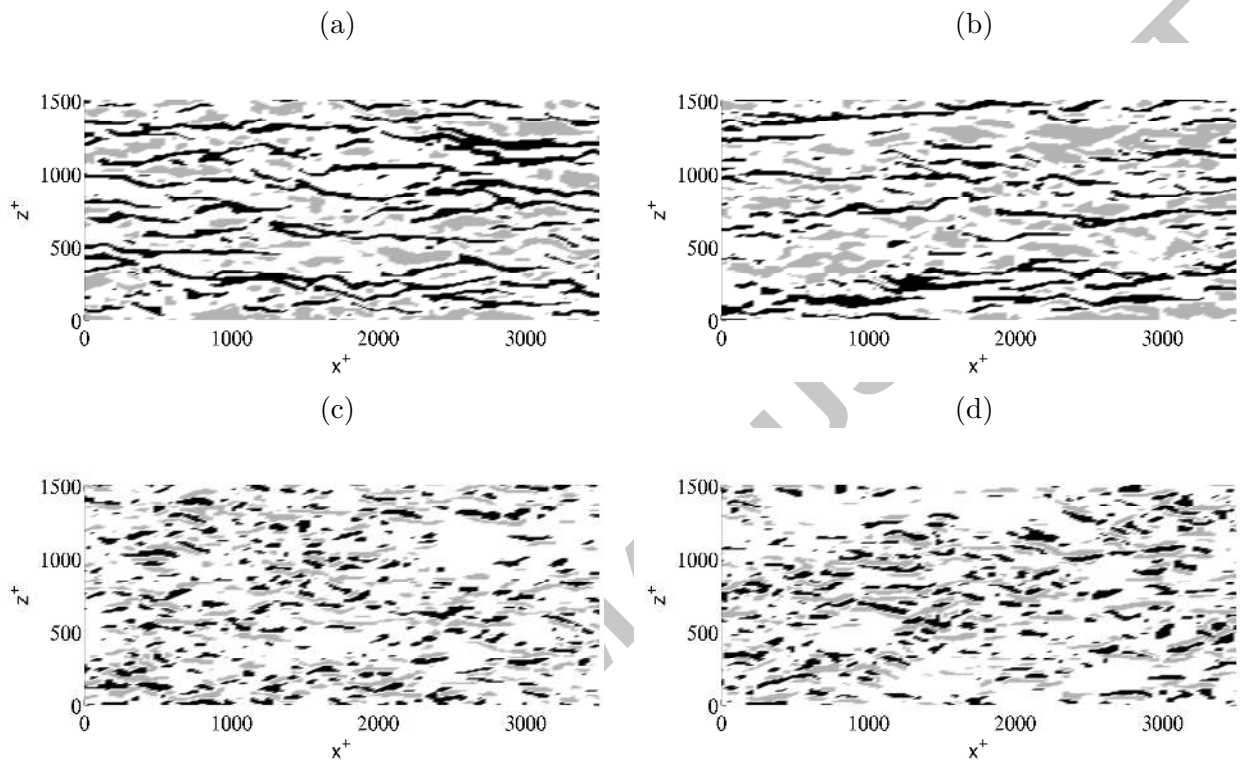


Figure 12. Snapshots of velocity fluctuations  $u$  and  $v$  obtained at the same time at  $y^+ = 18$ : (a,b) streamwise velocity (black:  $u < U - u_{rms}$ , white:  $U - u_{rms} < u < U + u_{rms}$ , grey:  $u > U + u_{rms}$ , where  $U$  is the mean streamwise velocity), (c,d) wall-normal velocity (black:  $v < -v_{rms}$ , white:  $-v_{rms} < v < v_{rms}$ , grey:  $v > v_{rms}$ ), from cases (a,c) Re600 and (b,d) Re960.

### 3.4 Mean and fluctuating velocity profiles

The profiles of mean streamwise velocity  $U^+ = U/u_\tau$  obtained in the Re350, Re600 and Re960 cases are presented in figure 13 as a function of the distance to the wall  $y^+ = yu_\tau/\nu$ . For  $y^+ \leq 100$ , the profiles are superimposed. They follow the mean velocity laws  $U^+ = f(y^+)$  typically found in turbulent boundary layers, represented by dots, namely the linear law  $U^+ = y^+$  for  $y^+ \leq 5$  in the viscous sublayer, and the logarithmic law  $U^+ = \ln(y^+)/\kappa + B$  with  $\kappa = 0.41$  and  $B = 5$  for  $30 < y^+ < 100$  in the so-called logarithmic layer. These values of  $\kappa$  and  $B$  fall within the range of values given by numerical and experimental studies [42].

For  $5 < y^+ < 30$ , the velocity profiles deviate from the two analytic curves. This is expected because this region, named the buffer layer, corresponds to a transition zone between the viscous sublayer and the logarithmic layer.

Finally, for  $y^+ \geq 100$ , the well-known outer-layer wake deviation of the mean velocity profile with respect to the logarithmic law is observed. Slight differences appear between the three LES, because the velocity profiles in this flow region scale with outer variables [41].

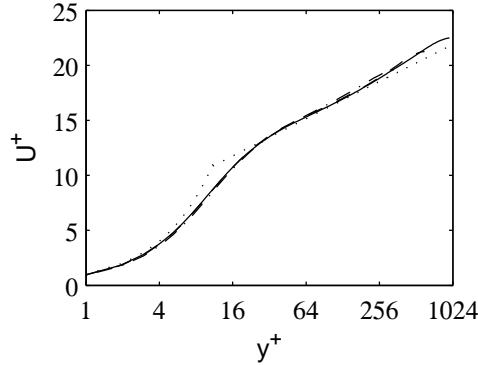


Figure 13. Representation of the mean streamwise velocity obtained from cases Re350, Re600 and Re960, as a function of the wall distance using wall units;  $U^+ = y^+$  for  $y^+ \leq 10$  and  $U^+ = \ln(y^+)/\kappa + B$  with  $\kappa = 0.41$  and  $B = 5$  for  $y^+ \geq 10$ .

The profiles of rms streamwise velocity fluctuations  $u_{rms}^+ = u_{rms}/u_\tau$  calculated from the Re350, Re600 and Re960 simulations are represented in figure 14(a) as a function of the distance to the wall  $y^+$  in wall units. They are very similar for  $5 \leq y^+ \leq 50$  in the buffer region. The peak of rms velocity is located at  $y^+ \simeq 14.5$ , and slightly increases with the Reynolds number, as observed, for example, in the DNS of Hu *et al.* [7] for channel flows at  $Re_\tau = 90 - 1440$ . Another change is noted for  $y^+ \geq 50$ , where the profiles present a hump growing in magnitude and shifting toward higher values of  $y^+$  as the Reynolds number increases.

The rms velocity profiles are re-plotted in figure 14(b) as a function of  $y/h$ . In that case, they strongly differ near the wall, whereas they are very close farther away for  $y/h > 0.2$ . In the outer flow region, the fluctuating streamwise velocity thus appears to follow a similarity law when a mixed scaling based on  $u_\tau$  for the velocity scale and  $h$  for the length scale is used.

### 3.5 Comparison with reference data

The mean and fluctuating velocity profiles obtained in the Re350, Re600 and Re960 cases are compared with the reference DNS data provided by Moser *et al.* [3] and del Alamo *et al.* [6] for turbulent channel flows at  $Re_\tau = 395, 590$  and  $950$ . These Reynolds numbers are not exactly identical to those of the LES, but they are fairly close to them, which should allow relevant comparisons to be made. It can be noted that the mesh spacings are significantly larger in the LES than those in the DNS, which are indicated in table 1. This leads to a substantial

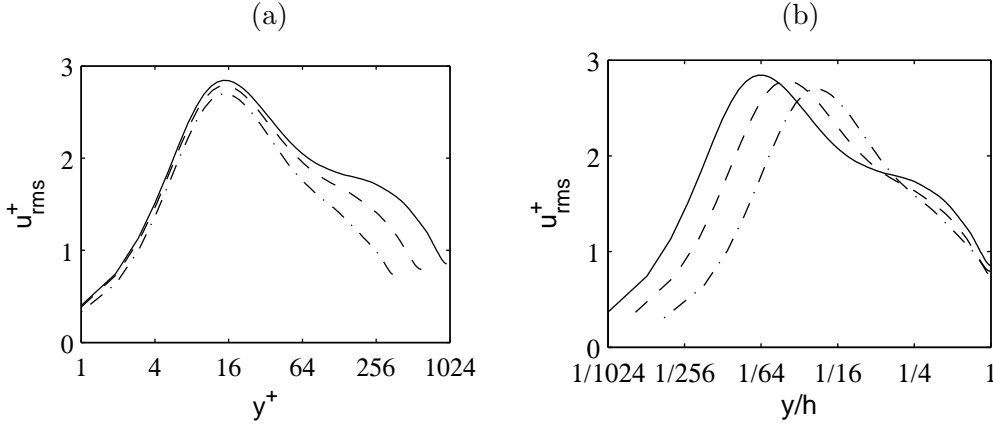


Figure 14. Representation of the rms streamwise velocity fluctuations  $u_{rms}^+$  obtained from cases Re350, Re600 and Re960, as a function of the wall distance (a)  $y^+$  and (b)  $y/h$ .

reduction in the number of grid points. For instance, the LES grid in the Re960 case contains 68 million points, when 2.7 billion points are used in the DNS of del Alamo *et al.* [6] at  $Re_\tau = 950$ .

The profiles of mean streamwise velocity and of rms streamwise, wall-normal and spanwise velocity fluctuations given by the Re350 computation and the DNS at  $Re_\tau = 395$  are presented in figure 15. The LES and DNS results are very similar for  $y^+ \leq 50$ . For larger distances to the wall, the fluctuation levels are slightly stronger in the DNS than in the LES, which may be due to the higher Reynolds number in the DNS. The mean and fluctuating velocity profiles from the Re600 simulation and the DNS at  $Re_\tau = 590$  are shown in figure 16. The agreement between the LES and the DNS results is excellent in all cases. In particular, the hump around  $y^+ = 200$  pointed out in section 3.4 in the LES profile of rms streamwise velocity fluctuations also appear in the DNS corresponding profile. Finally, the velocity profiles from the Re960 case and the DNS at  $Re_\tau = 960$  are given in figure 17. Here again, the LES and DNS results are in very good agreement.

These successful comparisons with DNS data demonstrate that the present LES of turbulent channel flows are reliable, and properly take into account Reynolds number effects both qualitatively and quantitatively.

### 3.6 Velocity spectra

Finally, power spectral densities  $\phi_{uu}$  of the streamwise velocity fluctuations are computed in the buffer region at a distance to the wall of  $y^+ = 18$  for the Re350, Re600 and Re960 cases. They are represented as a function of the spanwise wavenumber  $k_z$  in figure 18(a) using a normalization by inner scales. For low wavenumbers  $k_z^+ \leq 0.02$ , there are strong differences between the results

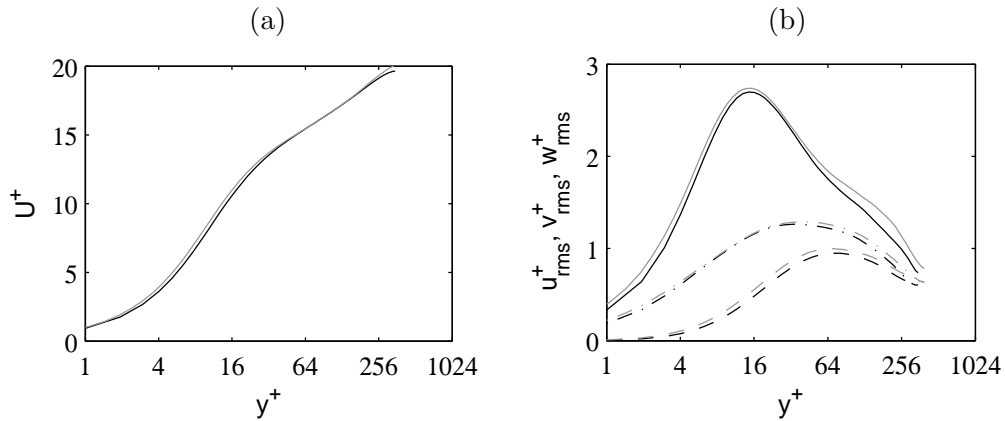


Figure 15. Representation (a) of the mean streamwise velocity and (b) the rms velocity fluctuations  $u_{rms}^+$ ,  $v_{rms}^+$  and  $w_{rms}^+$ , obtained from case Re350 and from grid the DNS of Moser *et al.* [3] at  $Re_\tau = 395$ , as a function of the wall distance using wall units.

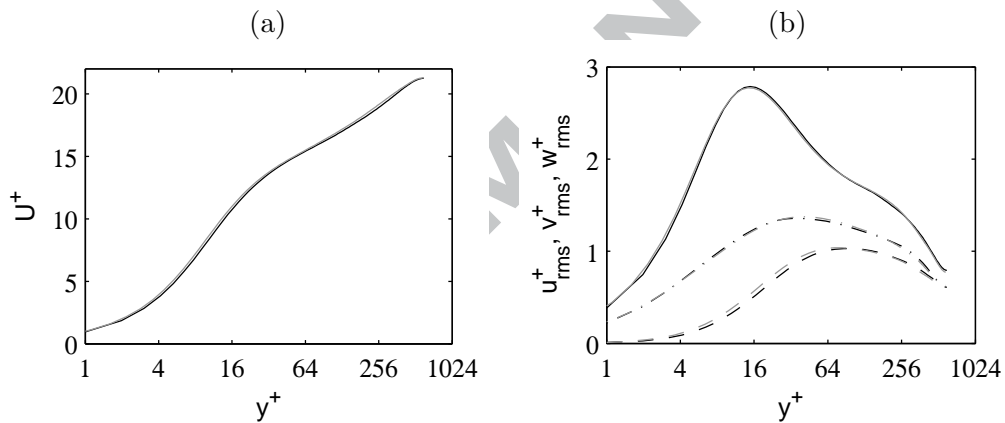


Figure 16. Representation (a) of the mean streamwise velocity and (b) the rms velocity fluctuations  $u_{rms}^+$ ,  $v_{rms}^+$  and  $w_{rms}^+$ , obtained from case Re600 and from grid the DNS of Moser *et al.* [3] at  $Re_\tau = 590$ , as a function of the wall distance using wall units.

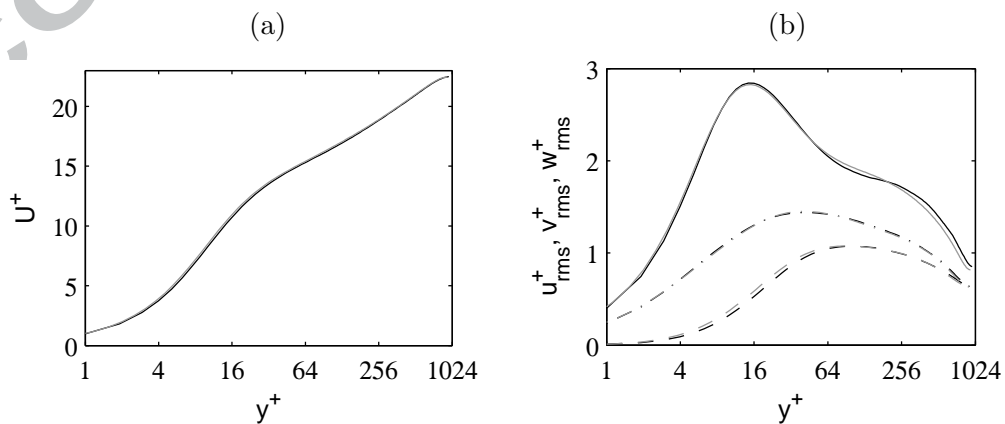


Figure 17. Representation (a) of the mean streamwise velocity and (b) the rms velocity fluctuations  $u_{rms}^+$ ,  $v_{rms}^+$  and  $w_{rms}^+$ , obtained from case Re960 and from grid the DNS of del Alamo *et al.* [6] at  $Re_\tau = 950$ , as a function of the wall distance using wall units.

from the three LES, which will be discussed below. For  $k_z^+ \geq 0.02$ , the spectra are very close, those from the Re600 and Re960 simulations even being superimposed. They are rather flat between  $k_z^+ = 0.02$  and 0.035, and decrease at higher wavenumbers. The slope of the curves does not vary much between  $k_z^+ \simeq 0.06$  and 0.15, and then becomes steeper. The latter collapse is due to the relaxation filtering, which affects wavelengths shorter than  $5\Delta z$ , corresponding to wavenumbers  $k_z^+ \geq 0.15$  for Re350 and  $k_z^+ \geq 0.12$  for Re600 and Re960.

The very good fit of the velocity spectra obtained at different Reynolds numbers for  $k_z^+ \geq 0.02$  in figure 18(a) using an inner normalization illustrates the independence of the small turbulent structures in the buffer region, namely the near-wall streaks, from the outer scales of the flow. The dominant components in this spectral region are located at  $k_z^+ = 0.02 - 0.035$ , which indicates that the spanwise scale of the most energetic streaks ranges from  $\lambda_z^+ = 180$  to 300. These values are higher than the spanwise separation of about 100 wall units classically found in the literature for turbulent boundary layers [43]. They are however similar to those measured by Tomkins & Adrian [44], who obtained dominant spanwise scales between  $\lambda_z^+ = 200$  and 400 in a turbulent boundary layer at  $Re_\tau = 426$ .

The results provided by the LES for low wavenumbers  $k_z^+ \leq 0.02$  are now examined. In this spectral region, strong components clearly emerge for  $k_z^+ = 0.003 - 0.005$  in the Re960 case and for  $k_z^+ = 0.005 - 0.01$  in the Re600 case, with magnitudes two times smaller in the second simulation. In the Re350 case, no significant peak is observed, and the levels are again two times smaller than those of the Re600 case. An higher Reynolds number thus results in the amplification of low-wavenumber components, which do not scale using wall units. On the contrary, when normalized using outer units as in figure 18(b), the spectra are in good agreement for spanwise wavenumbers in the range  $3 \leq k_z h \leq 6$ , corresponding to spanwise wavelengths  $h \leq \lambda_z \leq 2h$ . The low-wavenumber components are consequently related to the outer scales of the flow.

## 4 Conclusion

In this paper, LES of fully developed channel flows using relaxation filtering as subgrid model are reported. The simulations are performed using different grid resolutions and for various Reynolds numbers, in order to assess the validity of the LES approach for turbulent wall-bounded flows.

For the LES at a fixed Reynolds number  $Re_\tau = 300$  carried out with different spatial resolu-



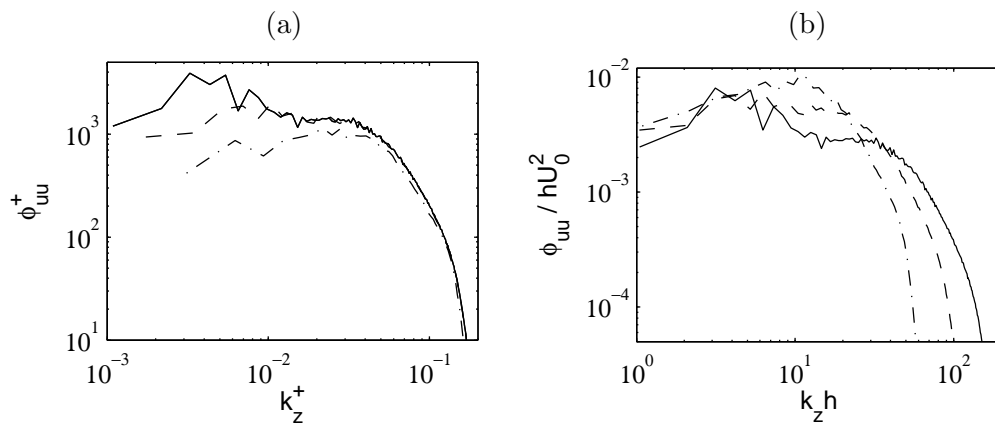


Figure 18. Representation of the power spectral densities of the streamwise velocity fluctuations obtained from cases Re350, Re600 and Re960 as a function of the spanwise wavenumber  $k_z$  using (a) inner units and (b) outer units.

tions, the mean and rms velocity profiles are found not to change significantly with the grid for mesh spacings  $\Delta x^+ \leq 30$  in the axial direction,  $\Delta y^+ \leq 1$  in the wall-normal direction at the wall and  $\Delta z^+ \leq 10$  in the spanwise direction, in wall units. The severe limitation on  $\Delta y^+$  at the wall is expected because of the need to take into account the small scales developing close to the wall. Based on the calculation of integral length scales and spectra, the constraint on  $\Delta z^+$  is shown to be due to the necessity to sufficiently discretize the scales dominating in the spanwise direction. In the present LES, more than 4 mesh spacings, which corresponds approximately to the limit above which the scales are not damped by the filtering, are required. Finally, the constraint on  $\Delta x^+$  is explained in the light of the dissipation transfer functions associated with molecular viscosity and relaxation filtering. It is indeed found that a part of the resolved turbulent scales may be affected by the filtering for  $\Delta x^+ \geq 30$  in the present simulations.

For the LES of channel flows at Reynolds numbers  $Re_\tau = 350, 600$  and  $960$  performed using fine grids, the results are shown to be reliable, and agree very well with DNS results of the literature. This demonstrates that the Reynolds number effects are well captured in the simulations. In particular, the emergence of a hump in the outer part of the profiles of rms velocity fluctuations as the Reynolds number increases is accurately reproduced. The shapes of the streamwise velocity spectra in the buffer region also change with the Reynolds number. High-wavenumber components in the spectra scale using inner units, whereas low-wavenumber components scale using outer units.

The present study indicates that the LES method based on relaxation filtering can be used to simulate fully turbulent wall-bounded flows, provided that, as should be the case in all

simulations, care is taken to ensure that grid resolution is sufficient and that largest scales are not overly affected by numerical dissipation.

## Acknowledgments

The first author is grateful to the Direction Générale de l'Armement (DGA) and the Centre National de la Recherche Scientifique (CNRS) for financial support for his doctoral studies. This work was granted access to the HPC resources of the Institut du Développement et des Ressources en Informatique Scientifique (IDRIS) under the allocation 2012-020204 made by GENCI (Grand Equipement National de Calcul Intensif). The authors would like to thank Olivier Marsden for his help in parallelizing the Navier-Stokes solver using OpenMP.

## References

- [1] Marusic I, McKeon BJ, Monkewitz PA, Nagib HM, Smits AJ, Sreenivasan KR. Wall-bounded turbulent flows at high Reynolds numbers: Recent advances and key issues. *Phys Fluids* 2010;22:065103.
- [2] Kim J, Moin P, Moser R. Turbulence statistics in fully developed channel flow at low Reynolds number. *J Fluid Mech* 1987;177:133-166.
- [3] Moser RD, Kim J, Mansour N. Direct numerical simulation of turbulent channel flow up to  $Re_\tau=590$ . *Phys Fluids* 1999;11(4):943-945.
- [4] Hu ZH, Morfey CL, Sandham ND. Aeroacoustics of wall-bounded turbulent flows. *AIAA J* 2002;40(3):465-473.
- [5] del Alamo JC, Jiménez J. Spectra of the very large anisotropic scales in turbulent channels. *Phys Fluids* 2003;15(6):L41-L44.
- [6] del Alamo JC, Jiménez J, Zandonade P, Moser RD. Scaling of the energy spectra of turbulent channels. *J Fluid Mech* 2004;500:135-144.
- [7] Hu ZH, Morfey CL, Sandham ND. Wall pressure and shear stress spectra from direct simulations of channel flow. *AIAA J* 2006;44(7):1541-1549.
- [8] Hoyas S, Jiménez J. Scaling of the velocity fluctuations in turbulent channels up to  $Re_\tau=2003$ . *Phys Fluids* 2006;18:011702.

- [9] Spalart PR. Direct simulation of a turbulent boundary layer up to  $Re_\theta=1410$ . *J Fluid Mech* 1988;187:61-98.
- [10] Schlatter P, Örlü R, Li Q, Brethouwer G, Fransson JHM, Johansson AV, Alfredsson PH, Henningson DS. Turbulent boundary layers up to  $Re_\theta=2500$  studied through simulation and experiment. *Phys Fluids* 2009;21:051702.
- [11] Simens MP, Jiménez J, Hoyas S, Mizuno M. A high-resolution code for turbulent boundary layers. *J Comput Phys* 2009;228(11):4218-4231.
- [12] Wu X, Moin P. Direct numerical simulation of turbulence in a nominally zero-pressure-gradient flat-plate boundary layer. *J Fluid Mech* 2009;630:5-41.
- [13] Schlatter P, Örlü R. Assessment of direct numerical simulation data of turbulent boundary layers. *J Fluid Mech* 2010;659:116-126.
- [14] Sagaut P. Large Eddy Simulation for incompressible flows - An introduction, third edition. Springer-Verlag, Scientific Computation series, 2005.
- [15] Piomelli U, Balaras E. Wall-layer models for large-eddy simulations. *Annu Rev Fluid Mech* 2002;34:349-374.
- [16] Chung D, McKeon BJ. Large-eddy simulation of large-scale structures in long channel flow. *J Fluid Mech* 2010;661:341-364.
- [17] Viazzo S, Dejoan A, Schiestel R. Spectral features of the wall-pressure fluctuations in turbulent wall flows with and without perturbations using LES. *Int J Heat Fluid Flow* 2001;22:39-52.
- [18] Suh J, Frankel SH, Mongeau L, Plesniak MW. Compressible large eddy simulations of wall-bounded turbulent flows using a semi-implicit numerical scheme for low Mach number aeroacoustics. *J Comput Phys* 2006;215(2):526-551.
- [19] Gloerfelt X, Berland J. Turbulent boundary layer noise: direct radiation at Mach number 0.5 *J Fluid Mech* 2012;723:318-351.
- [20] Schlatter P, Li Q, Brethouwer G, Johansson AV, and Henningson DS. Simulations of spatially evolving turbulent boundary layers up to  $Re_\tau = 4300$ . *Int J Heat Fluid Flow* 2010;31:251-261.

- [21] Schlatter P, Örlü R. Turbulent boundary layers at moderate Reynolds numbers: inflow length and tripping effects. *J Fluid Mech* 2012;710:5-34.
- [22] Rasam A, Brethouwer G, Schlatter P, Li Q, Johansson AV. Effects of modelling, resolution and anisotropy of subgrid-scales on large eddy simulations of channel flow. *J Turbulence* 2010;12(10):1-20.
- [23] Vuorinen V, Larmi M, Schlatter P, Fuchs L, Boersma BJ. A low-dissipative, scale-selective discretization scheme for the Navier-Stokes equations. *Comput Fluids* 2011;70:195-205.
- [24] Visbal MR, Rizzetta DP. Large-Eddy Simulation on curvilinear grids using compact differencing and filtering schemes. *J Fluids Eng* 2002; 124(4):836-847.
- [25] Mathew J, Lechner R, Foysi H, Sesterhenn J, Friedrich R. An explicit filtering method for large eddy simulation of compressible flows. *Phys Fluids* 2003;15(8):2279-2289.
- [26] Bogey C, Bailly C. Large Eddy Simulations of transitional round jets: influence of the Reynolds number on flow development and energy dissipation. *Phys Fluids* 2006;18(6):065101.
- [27] Tantikul T, Domaradzki JA. Large-eddy simulations using truncated Navier-Stokes equations with the automatic filtering criterion. *J Turbulence* 2010;11(21):1-24.
- [28] Fauconnier D, Bogey C, Dick E. On the performance of relaxation filtering for large-eddy simulation. *J Turbulence* 2013;14(1):22-49.
- [29] Berland J, Lafon P, Daude F, Crouzet F, Bogey C, Bailly C. Filter shape dependence and effective scale separation in large-eddy simulations based on relaxation filtering. *Comput Fluids* 2011;47(1):65-74.
- [30] Bogey C, Bailly C. Large eddy simulations of round free jets using explicit filtering with/without dynamic Smagorinsky model. *Int J Heat Fluid Flow* 2006;27:603-610.
- [31] Bogey C, Bailly C. Turbulence and energy budget in a self-preserving round jet: direct evaluation using large eddy simulation. *J Fluid Mech* 2009;627:129-160.
- [32] Bogey C, Marsden O, Bailly C. Large-Eddy Simulation of the flow and acoustic fields of a Reynolds number  $10^5$  subsonic jet with tripped exit boundary layers. *Phys Fluids* 2011;23:035104.

- [33] Marden O, Bogey C, Bailly C. Direct noise computation of the turbulent flow around a zero-incidence airfoil. *AIAA J* 2008;46(4):874-883.
- [34] Bogey C, Marsden O, Bailly C. Effects of moderate Reynolds numbers on subsonic round jets with highly disturbed nozzle-exit boundary layers. *Phys Fluids* 2012;24:105107.
- [35] Bogey C, Bailly C. A family of low dispersive and low dissipative explicit schemes for flow and noise computations. *J Comput Phys* 2004;194(1):194-214.
- [36] Berland J, Bogey C, Bailly C. Low-dissipation and low-dispersion 4th-order Runge-Kutta algorithm. *Comput Fluids* 2006;35:1459-1463.
- [37] Bogey C, de Cacqueray N, Bailly C. A shock-capturing methodology based on adaptive spatial filtering for high-order non-linear computations. *J Comput Phys* 2009;228(5):1447-1465.
- [38] Kremer F, Bogey C, Bailly C. Semi-implicit Runge-Kutta schemes: development and application to compressible channel flow. *AIAA J* 2014;52(3):515-527.
- [39] Robinson SK. A review of vortex structures and associated coherent motions in turbulent boundary layers. *Annu Rev Fluid Mech* 1991;23:601-39.
- [40] Jiménez J, del Alamo JC, Flores O. The large-scale dynamics of near-wall turbulence. *J Fluid Mech* 2004;505:179-199.
- [41] Coles D. The law of the wake in the turbulent boundary layer. *J Fluid Mech* 1956;1:191-226.
- [42] Nagib HM, Chauhan KA. Variations of von Kármán coefficient in canonical flows. *Phys Fluids* 2008;20:101518.
- [43] Kline SJ, Reynolds WC, Schraub FA, Runstadler PW. The structure of turbulent boundary layers. *J Fluid Mech* 1967;30:741-773.
- [44] Tomkins CD, Adrian RJ. Energetic spanwise modes in the logarithmic layer of a turbulent boundary layer. *J Fluid Mech* 2005;545:141-162.
- [45] Wei L, Pollard A. Direct numerical simulation of compressible turbulent channel flows using the discontinuous Galerkin method. *Comput Fluids* 2011;47:85-100.

# Large-eddy simulation of turbulent channel flow using relaxation filtering: resolution requirement and Reynolds number effects

Francois Kremer\* and Christophe Bogey†

*Laboratoire de Mécanique des Fluides et d'Acoustique, UMR CNRS 5509,  
Ecole Centrale de Lyon, Université de Lyon, 69134 Ecully Cedex, France*

March 28, 2014

## Highlights

- LES of channel flows are performed for different grids and Reynolds numbers
- the performance of the LES method using relaxation filtering is thus assessed
- good agreement is found with Direct Numerical Simulation results
- the LES results are shown to converge with decreasing the mesh spacings
- Reynolds number effects are shown to be well captured in the LES

---

\*PhD, Email: kremer.francois@ec-lyon.fr

†CNRS Research Scientist, Email: christophe.bogey@ec-lyon.fr